Using Terahertz Spectroscopy to Study Nanomaterials

Charles A. Schmuttenmaer
Yale University, Department of Chemistry, 225 Prospect St.,
P. O. Box 208107, New Haven, CT 06520-8107, USA
Email: charles.schmuttenmaer@yale.edu

Abstract: The microscopic details of carrier transport in nanocrystalline colloidal thin films is required for complete understanding of a variety of photochemical and photoelectrochemical cells utilizing interpenetrating networks. Measuring the photoconductivity and charge transport properties in these materials, however, is a challenging problem because of the inherent difficulty of attaching wires to nanometer-sized objects. Furthermore, picosecond (ps) carrier dynamics play an important role in efficient charge separation and transport, but the low temporal resolution of traditional methods used to determine the photoconductivity precludes their use in studying sub-ps to ps dynamics. Time-resolved THz spectroscopy (TRTS), on the other hand, is a non-contact electrical probe capable of measuring the photoconductivity on a sub-ps to nanosecond (ns) timescale. In this talk, TRTS is employed to determine the transient photoconductivity of ZnO nanowires, polycrystalline, and nanoparticle films, as well as dye-sensitized nanocrystalline colloidal TiO2 films. Electron injection occurs on sub-ps time scales. Decay kinetics (on hundreds of ps to ns time scales) indicate that surfaces and interfaces are the dominant sources of recombination. The photoconductivity deviates strongly from Drude behavior and is explained by disorder-induced carrier localization and/or backscattering of the photogenerated carriers. Trends as a function of material and morphology will be discussed.

I. Introduction

The photoconductivity and charge transport properties of semiconductor nanoparticles (NPs) are critically important with regard to their use in electro-optic devices.[1] Similarly, understanding the microscopic details of carrier transport in nanocrystalline colloidal thin films is required for complete understanding of a variety of photochemical and photoelectrochemical cells utilizing interpenetrating networks. Measuring the photoconductivity in these materials, however, is a challenging problem because of the inherent difficulty of attaching wires to nanometer-sized objects. Furthermore, picosecond (ps) carrier dynamics play an important role in efficient charge separation and transport, but the low temporal resolution of traditional methods used to determine their photoconductivity precludes their use in studying sub-ps to ps dynamics.

Time-resolved THz spectroscopy (TRTS), on the other hand, is a non-contact electrical probe capable of measuring the photoconductivity on a sub-ps to nanosecond (ns) timescale.[2, 3] In essence, materials with high conductivity strongly absorb THz radiation, while those with low conductivity do not. With THz spectroscopy, not only can the average time-dependent conductivity properties be measured, but also the complete frequency-dependent, complex-valued conductivity (i.e., real and imaginary components), all on a sub-ps timescale, and without attaching any probe wires to the sample. In this paper, TRTS is employed to study the transient photoconductivity in nanocrystalline colloidal TiO_2 and ZnO nanoparticles, ZnO nanowires, and CdSe NPs of various sizes.

II. Experimental Methods

TiO$_2$ and ZnO NPs were spin-coated, and the CdSe quantum dots (QDs) were drop-cast. ZnO nanowires and films were grown on glass cover slips by chemical bath deposition from zinc nitrate and methenamine.[4]   After three hours, nanowires have lengths of ~1 μm and diameters of 50-100 nm.   It is possible to further increase the nanowire aspect ratio by placing the nanowire substrate into a fresh batch of precursor solution and repeating the deposition process, now using the nanowires themselves as seeds.   By repeating this process for eight growth cycles, we have grown nanowires up to 8 μm long with diameters under 200 nm.

The THz system has been described in detail previously.[3]   The pump/probe aspect of the experiment is shown schematically in Figure 1.   By collecting a THz probe pulse over a range of times after photoexcitation of the sample, we monitor the change in optical constants (absorption coefficient and refractive index) of the sample.   These changes are directly related to changes in the sample's conductivity.[3]   Figure 2 shows the scans that must be collected.   The optical constants of the glass microscope slide cover slip on which the sample is deposited are obtained by comparing the black and red scans.   The ZnO constants are obtained by comparing the green and red scans.   The photoexcited ZnO optical constants are obtained by comparing the dark blue and green scans.   For samples that absorb only very weakly, the THz difference scan is taken, shown with the light blue line, while modulating the photoexcitation beam with an optical chopper.
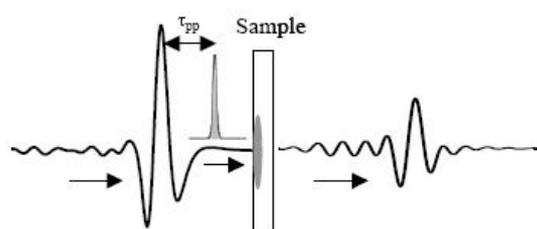

Figure 1.   Schematic illustration of the effect of photoexcitation on the transmitted THz pulse.   The entire waveform can be analyzed to obtain the frequency dependent complex conductivity, or the maximum point on the THz waveform can be recorded as a function of pump-probe delay time to measure the average conductivity as a function of time, and this is known as a THz "pump scan".
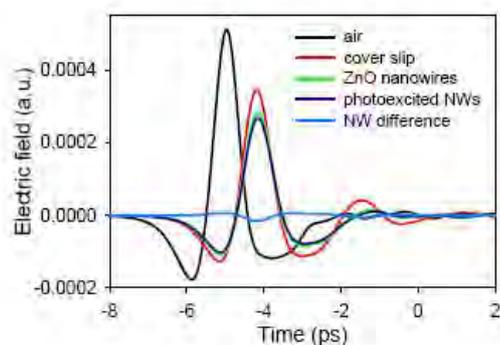

Figure 2.   The black line is the THz pulse with no sample in the beam path.   The red line shows the effect of the glass cover slip on the THz pulse.   The green line is that of the ZnO nanowires on top of the glass cover slip.   The dark blue line shows the THz transmission after photoexcitation of the ZnO sample.   The light blue line is the THz "difference scan" when a chopper is placed in the excitation laser beam path, and a lockin amplifier is used.

III. Nanocrystalline TiO$_2$ and ZnO

Colloidal sintered TiO$_2$ forms the heart of the so-called "Grätzel cell", a type of dye-sensitized solar cell that has attracted attention since 1991.[5] Most of the ultrafast spectroscopy done on this system has focused on the dye molecule.   That is, one observes a sharp reduction in fluorescence quantum yield and lifetime when the molecule is adsorbed to TiO$_2$ compared to when it is in solution.   This behavior is attributed to rapid electron injection upon photoexcitation.

The TiO$_2$ nanoparticles in a DSSC are sintered together to enable interparticle charge transport through the device, which is believed to proceed via a hopping mechanism over a distribution of barrier heights.[6-9]   Until now, the details of this transport have not been fully characterized.

The measured conductivity 3 ps after photoexcitation of dye-sensitized nanocrystalline TiO$_2$ is shown in Figure 3, and remains unchanged for delay times up to at least 1 ns.   The deviation from Drude behavior (shown with the dashed lines) is striking: the real part of the conductivity increases with increasing frequency, and the imaginary part of the conductivity is *negative*.   It is mathematically impossible for the Drude model and its simple variants to reproduce this behavior. The photoconductivity in bulk single-crystal rutile TiO$_2$ and ZnO at 77 K are in fact well described by the Drude model,[10-12] yielding a scattering time of $\tau = 320$ fs, indicating that there is something fundamentally different with nanocrystalline materials.
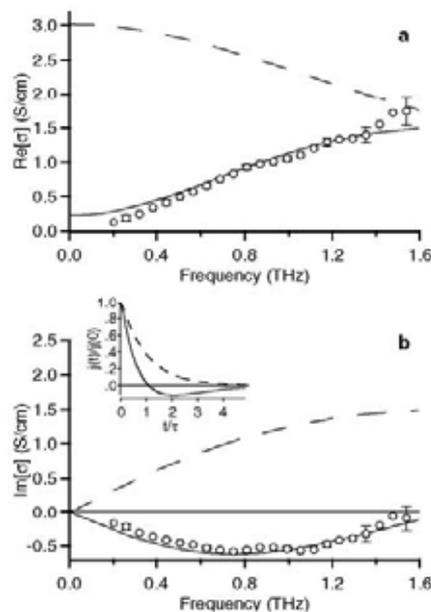

Figure 3. Experimentally determined real (a) and imaginary (b) parts of the conductivity at 77 K in unsintered TiO$_2$ sensitized with Ru535. Open circles are representative data taken 3 ps after photoexcitation, with the best fit of the Smith model shown as a solid line.   The Drude conductivity is shown for comparison (dashedline).   Parameters for the Drude-Smith model are: $\omega_p = 20.7$ x 10^{12} s^{-1}, $\tau = 84$ fs, and $c = -0.93$. The inset shows the current impulse response function, $j(t)/j(0)$, for the Drude-Smith model with $c = -0.93$ (solid line) and Drude model (dashed line).

Smith proposed a classical modification to the Drude model that allows for a significant deviation from the general Drude features described above.[13] The functional form of the model describes the complex conductivity $\hat{\sigma}(\omega)$ as

$$\hat{\sigma}(\omega) = \frac{\varepsilon_o \omega_p^2 \tau}{(1 - i\omega\tau)}\left[1 + \frac{c}{(1 - i\omega\tau)}\right].$$
 (1)

It consists of the basic Drude model, plus an additional term, c, that accounts for the fraction of the carrier's initial velocity retained after experiencing a collision. The free-space permittivity is ε_o, τ is the carrier collision time, $\omega = 2\pi\nu$ is the radial frequency, and the plasma frequency is given by $\omega_p^2 = Ne^2/(\varepsilon_o m^*)$, where N is the carrier density and m^* is the carrier effective mass. When $c = 0$, the standard Drude model is obtained. When $c = -1$, the real part of the conductivity is 0 at dc and the imaginary part of the conductivity is negative at low frequencies as seen in Figure 3. This is interpreted as conductivity dominated by backscattering.[13] Values of c near –1 result in small fractional current displacements and small (but non-zero) dc conductivity. Smith's model best represents our data when $c \approx -0.9$, as indicated by the best fit to the data shown in Figure 3.

We performed a global fit of the transient conductivity as a function of time after photoexcitation. The results are shown in Figure 4. The c parameter begins near a value of –0.5, and decreases to about –0.9 on a 300 fs timescale. The scattering time increases from about 40 fs to 80 fs, also on a 300 fs timescale. Thus, the carriers are more Drude-like, but scattering rapidly at early times, and become dominated by localization after they have thermalized with the lattice.

Another commonly used method to treat composite media is the Bruggemen effective medium theory.[12, 14, 15] When a conductor/nonconductor composite is close to the percolation threshold, it is possible for the real and imaginary conductivity to behave in the manner that we have measured. However, unlike the Drude-Smith model, effective medium theory can not reproduce the data immediately after photoexcitation. Thus, a global fit using this model was not performed.

These TRTS results demonstrate that the carriers within TiO_2 nanoparticles deviate from their bulk Drude-like behavior. However, at short length scales the carriers are still quite mobile, with longer-range transport hindered by disorder. We have provided an unprecedented level of detail about the microscopic nature of charge transport in nanocrystalline TiO_2 films. By measuring the frequency-dependent complex-conductivity on a sub-picosecond time scale, we have shown that carrier cooling within the conduction band occurs in about 300 fs. These observations are consistent with the present understanding of dc transport in actual DSSC assemblies, and provide new insight into the nature of the conduction mechanism. It is now clear that electrons within nanoparticles are quite mobile, yet their bulk transport is hindered by disorder.
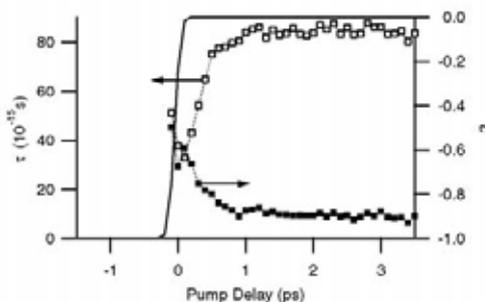
Figure 4.   Plot of the carrier scattering time τ(open squares) and *c* (solid squares) as a function of pump delay time based on global fit described in Ref. 10.   The solid line indicates the onset of photoconductivity.
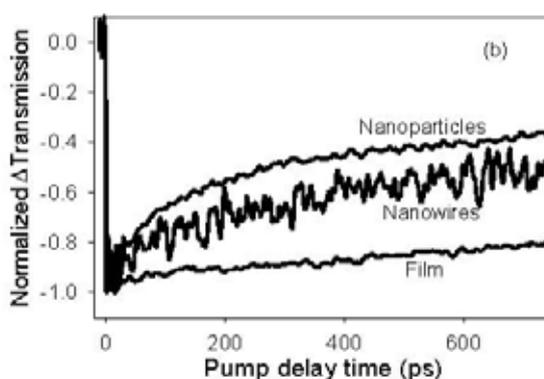

Figure 5. Decrease in photoconductivity as afunction of pump-probe delay time for various ZnOmorphologies.

Figure 5 displays THz "pump scans", which provide the change in overall conductivity as a function of pump-probe delay time, for 3 different ZnO morphologies.   It is seen that the nanoparticles, which have the highest surface area to volume ratio, display the fastest carrier trapping and/or recombination, while the continuous polycrystalline ZnO films have very little trapping and/or recombination on a ns time scale, and the ZnO nanowires, which have intermediate surface area, have an intermediate amount of trapping and/or recombination.   A more detailed analysis of the ZnO results is presented in Reference 4.

IV. CdSe Quantum Dots

Semiconductor NPs have sustained tremendous interest in the chemistry and physics communities because of dramatic size-dependent effects.   As the physical dimensions of NPs approach molecular dimensions, quantization effects become important and many bulk properties become size-dependent.   The most well documented example is that the bandgap increases as the particle size decreases, shifting the absorption and luminescence spectra to the blue.[16, 17] Size-dependent redox potentials,[18] lattice constants, fluorescence Stokes shifts,[19] and phase transitions, such as the pressure induced structural transition,[20] and melting point[21] have also been

observed.

Nearly monodisperse samples with sizes ranging from 2.54 nm to 25 nm were prepared by the method developed by Peng *et al*.[22, 23] The goal of our work is to investigate the size-dependent photoconductivity in semiconductor NPs. Figure 6 displays THz "pump scans" of several different sizes of NPs. As is the case for the ZnO samples, it is seen that carrier trapping and/or recombination is fastest for the smallest particles, and slowest for the largest particles.

We also analyzed the full frequency-dependent complex conductivity to extract the carrier mobility within the NPs. The conductivity is affected primarily by two fundamental length scales: the Bohr exciton radius a_B, and the carrier mean free path l_f. The Bohr exciton radius describes the spatial extent of the *e-h* pair and is defined as $a_B = \hbar^2 \varepsilon /(m^*e^2)$ where m^* is the effective mass of the exciton, and ε is the dielectric constant.[24] For CdSe, $a_B = 4.9$ nm based on an electron effective mass of 0.13 m_e and a hole effective mass of 0.45 m_e.[25] Quantum size effects are most pronounced when the size of the NPs becomes smaller than a_B because of the physical confinement of the *e-h* pair. At these sizes, carrier transport within the NPs in the traditional sense is no longer a meaningful concept as the electron is delocalized over the entire NP. However, we expect a smooth transition from bulk behavior to that of the confined system.

At NP diameters smaller than or comparable to l_f there is an effective mean free path given by[26]

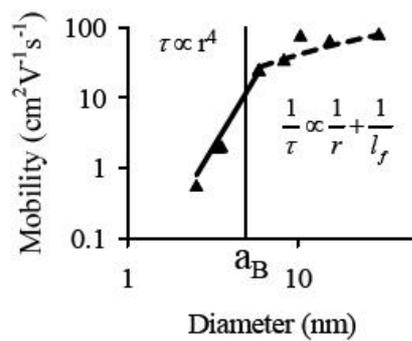$$\frac{1}{l_{eff}} = \frac{1}{r} + \frac{1}{l_f}. \qquad (2)$$

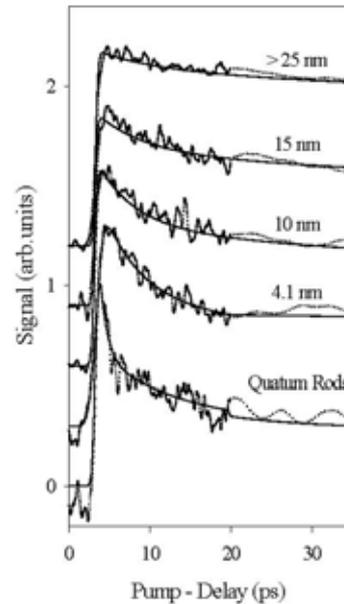**Figure 7.** Mobility in CdSe NPs as a function of size.

Figure 6. 1D pump delay scans of CdSe quantum dots of various sizes. Smooth curves are triple-exponential fits.

If we assume the velocity of the carriers remains the same as that in the bulk, then the scattering time is decreased: $\tau' = l_{eff}/v$ and this manifests itself as a reduction in the mobility, $\mu' = e\tau'/m^*$. Therefore, as the NP diameter decreases, the mobility should decrease with a dependence given by $\mu' \quad rl_f/(r + l_f)$. As seen in Figure 7, this dependence is observed for NPs larger than a_B. For smaller particles, the scattering time and mobility increase as r^4.

V. Conclusions

Terahertz spectroscopy can obtain carrier mobilities in bulk samples as well as nanostructured samples. The latter capability is particularly important because it is very difficult to attach wires to nanoscale particles. More importantly, when coupled with an ultrafast photoexcitation laser, i.e., when performing TRTS, it is possible to monitor the carrier mobility as it evolves as a function of time after photoexcitation.

References

[1] A. J. Nozik, Spectroscopy and hot electron relaxation dynamics in semiconductor quantum wells and quantum dots, *Annu. Rev. Phys. Chem.*, 52, 193-231, (2001).

[2] M. C. Beard, G. M. Turner and C. A. Schmuttenmaer, Subpicosecond carrier dynamics in low-temperature grown GaAs as measured by time-resolved terahertz spectroscopy, *J. Appl. Phys.*, 90, 5915-5923, (2001).

[3] M. C. Beard, G. M. Turner and C. A. Schmuttenmaer, Transient photoconductivity in GaAs as measured by time-resolved terahertz spectroscopy, *Phys. Rev. B*, 62, 15764-15777, (2000).

[4] J. B. Baxter and C. A. Schmuttenmaer, Conductivity of ZnO nanowires, nanoparticles, and thin films using time-resolved terahertz spectroscopy, *J. Phys. Chem. B*, 110, 25229-25239, (2006).

[5] B. O'Regan and M. Gratzel, A Low-Cost, High-Efficiency Solar-Cell Based On Dye-Sensitized Colloidal Tio2 Films, *Nature*, 353, 737-740, (1991).

[6] J. Nelson, Continuous-time random-walk model of electron transport in nanocrystalline TiO2 electrodes, *Phys. Rev. B*, 59, 15374-15380, (1999).

[7] J. Nelson, S. A. Haque, D. R. Klug and J. R. Durrant, Trap-limited recombination in dye-sensitized nanocrystalline metal oxide electrodes, *Phys. Rev. B*, 63, art. no. 205321, (2001).

[8] A. Hagfeldt and M. Gratzel, Molecular photovoltaics, *Accounts Chem. Res.*, 33, 269-277, (2000).

[9] M. Gratzel, Photoelectrochemical cells, *Nature*, 414, 338-344, (2001).

[10] G. M. Turner, M. C. Beard and C. A. Schmuttenmaer, Carrier localization and cooling in dye-sensitized nanocrystalline titanium dioxide, *J. Phys. Chem. B*, 106, 11716-11719, (2002).

[11] E. Hendry*, et al.*, Electron transport in TiO2 probed by THz time-domain spectroscopy, *Phys. Rev. B*, 69, (2004).

[12] E. Hendry, *Charge Dynamics in Novel Semiconductors*, University of Amsterdam, (2005).

[13] N. V. Smith, Classical generalization of the Drude formula for the optical conductivity, *Phys. Rev. B*, 64,

155106-+, (2001).

[14] D. Stroud, Percolation Effects and Sum-Rules in the Optical-Properties of Composites, *Phys. Rev. B*, 19, 1783-1791, (1979).

[15] E. Hendry, M. Koeberg, B. O'Regan and M. Bonn, Local field effects on electron transport in nanostructured TiO2 revealed by terahertz spectroscopy, *Nano Lett.*, 6, 755-759, (2006).

[16] A. L. Efros, Interband Absorption of Light in a Semiconductor Sphere, *Sov. Phys. Semicond.*, 16, 772-775, (1982).

[17] L. E. Brus, Electron Electron and Electron-Hole Interactions in Small Semiconductor Crystallites - the Size Dependence of the Lowest Excited Electronic State, *J. Chem. Phys.*, 80, 4403-4409, (1984).

[18] L. E. Brus, A Simple-Model For the Ionization-Potential, Electron-Affinity, and Aqueous Redox Potentials of Small Semiconductor Crystallites, *J. Chem. Phys.*, 79, 5566-5571, (1983).

[19] D. J. Norris, *Measurement and Assignment of the Size-Dependent Optical Spectrum in Cadmium Selenide (CdSe) Quantum Dots*, in *Chemistry*. Boston: Massachusetts Institute of Technology, 157, (1995).

[20] S. H. Tolbert and A. P. Alivisatos, Size Dependence of a First-Order Solid-Solid Phase-Transition - the Wurtzite to Rock-Salt Transformation in Cdse Nanocrystals, *Science*, 265, 373-376, (1994).

[21] A. N. Goldstein, C. M. Echer and A. P. Alivisatos, Melting in Semiconductor Nanocrystals, *Science*, 256, 1425-1427, (1992).

[22] L. Qu, Z. A. Peng and X. Peng, Alternative Routes toward High Quality CdSe Nanocrystals, *Nano Lett.*, 1, 333-337, (2001).

[23] Z. A. Peng and X. G. Peng, Formation of high-quality CdTe, CdSe, and CdS nanocrystals using CdO as precursor, *J. Am. Chem. Soc.*, 123, 183-184, (2001).

[24] J. R. Heath and J. J. Shiang, Covalency in semiconductor quantum dots, *Chem. Soc. Rev.*, 27, 65-71, (1998).

[25] S. V. Gaponenko, *Optical Properties of Semiconductor Nanocrystals*, New York: Cambridge University Press, (1998).

[26] N. W. Ashcroft and N. D. Mermin, *Solid State Physics*, New York: Saunders College Publishing, (1976).